IEEE Access
Multidisciplinary ⋮ Rapid Review ⋮ Open Access Journal

Received December 3, 2020, accepted December 18, 2020, date of publication December 22, 2020,
date of current version December 31, 2020.

Digital Object Identifier 10.1109/ACCESS.2020.3046656

IoT-Based Laser-Inscribed Sensors for Detection of Sulfate in Water Bodies

SHAN HE[1,2], SHILUN FENG[3,4], ANINDYA NAG[5], (Member, IEEE), NASRIN AFSARIMANESH[6], MD. ESHRAT E ALAHI[7], (Member, IEEE), SIYING LI[1], SUBHAS CHANDRA MUKHOPADHYAY[8], (Fellow, IEEE), AND JONATHAN WOON CHUNG WONG[9]

[1]School of Chemistry and Chemical Engineering, Guangzhou University, Guangzhou 510700, China
[2]Institute for NanoScale Scale Science and Technology, College of Science and Engineering, Flinders University, Bedford Park, SA 5042, Australia
[3]State Key Laboratory of Transducer Technology, Shanghai Institute of Microsystem and Information Technology, Chinese Academy of Sciences, Shanghai 518055, China
[4]School of Electrical and Electronic Engineering, Nanyang Technological University, Singapore 639798
[5]Department of Electrical engineering, CEMSE Division, King Abdullah University of Science of Technology, Thuwal 23955, Saudi Arabia
[6]DGUT-CNAM Institute, Dongguan University of Technology, Dongguan 523106, China
[7]Shenzhen Institutes of Advanced Technology, Chinese Academy of Sciences, Shenzhen 518055, China
[8]School of Engineering, Faculty of Science and Engineering, Macquarie University, Sydney, NSW 2109, Australia
[9]Institute of Bioresource and Agriculture, Hong Kong Baptist University, Hong Kong, China

Corresponding author: Anindya Nag (anindya1991@gmail.com)

This work was supported in part by the National Natural Science Fund from the National Science Foundation of China (NSFC) under Grant 61950410613, and in part by the CAS President International Fellowship Initiative from the Chinese Academy of Sciences under Grant 2019PT0008.

ABSTRACT This paper presents the fabrication of novel flexible sensors from metalized polymer films and their subsequent utilization for environmental applications. Polyethylene terephthalate films coated with thin-film of aluminum was used as a singular material to form the sensor patches. Optimization was done on the laser parameters to form laser-inscribed interdigitated electrodes on the aluminum side of the polymer films. The sensors were then used to detect the presence of sulfate ions in the water samples. Electrochemical impedance spectroscopy was used to detect the resistive and reactive changes with respect to the corresponding changes in the concentration of the tested solutions. Experiments were conducted using five different concentrations ranging between 0.1 ppm and 1000 ppm. The sensitivity, limit of detection and response time of the salts were 0.874 Ω/ppm, 0.1 ppm and one second, respectively. The repeatability of the sensors was also tested to validate their responses for the target analyte. An optimal frequency was chosen to form an IoT-based system that consisted of an impedance analyzer AD 5933, Wi-Fi embedded Arduino and 2:1 multiplexer ADG849. The interfacing of the microcontroller-sensed data was also done with the cloud server to showcase the potentiality of the developed systems as portable devices for real-time applications.

INDEX TERMS Laser-inscription, PET, aluminum, sulfate, microcontroller.

I. INTRODUCTION

The utilization of sensors for ubiquitous monitoring purposes has become commonplace over the last two decades [1], [2]. Different kinds of sensors have been fabricated using various processing materials, fabrication techniques, and sensor dimensions for multiple applications. For every case, the performance depends on specific attributes such as their input power, sensitivity, functionality, compatibility with the designated application, and the fabrication cost of the sensors. Earlier, with the popularisation of semiconducting sensors, silicon sensors were primarily used for monitoring domestic [3], [4], industrial [5], [6], and environmental [7], [8] applications. Even though the silicon sensors were capable of performing ubiquitously, certain disadvantages, including the high cost of fabrication, the requirement of high input power, and non-linearity in their responses, led researchers to seek suitable alternatives [9], [10]. Other disadvantages are their multi-step fabrication process that requires cleanroom facilities, generation of toxic fumes during the formation of the single-crystal sensors which cause health hazards and chronic diseases, a high signal-to-noise ratio at low frequencies, changes in their responses with respect to the change in ambient temperature, very low variation in response which

The associate editor coordinating the review of this manuscript and approving it for publication was Yongquan Sun.

consequently might need the conditioning circuits to amplify the signal, and high power consumption [11], [12]. Some of these disadvantages were being addressed by flexible sensors, thus making them quite expedient to be employed. These flexible sensors had additional advantages of low-cost fabrication techniques, simple operating principle, and enhanced electromechanical attributes. This paper outlines the single-step fabrication of flexible sensors using a singular material.

The application of the sensors primarily decides the type of raw material that can be processed with different fabrication techniques. Some of the conventional polymers that are being used to produce flexible prototypes are polydimethylsiloxane (PDMS) [13], [14], polyethylene terephthalate (PET) [15], [16], and polyimide (PI) [17], [18]. Their mechanical attributes, such as Young's Modulus (E), and electrical characteristics like interfacial bonding with the nano-fillers, are the main reasons for using these polymers. PET is one of the popular polymers primarily used to form sensing prototypes [19]–[21] due to its lightweight, high flexibility, high robustness, and high resistance towards chemicals. Among the different techniques that exploit PET to form sensors, the employment of metalized PET films [22], [23] is an efficient method where a single material is processed to synthesize the electrodes and the substrates of the sensor. The thickness of the electrodes and substrates depends on the type of metalized PET films being processed. Other advantages of using these metalized films include quick fabrication, high robustness due to its consisting of a single element and easy customization of the sensor design. Among the range of fabrication techniques that have been utilized to develop the flexible sensors, laser inscription [24]–[26] has been very effective in recent years. Some of the advantages associated with this process are non-contact process, low power consumption, formation of very thin-film cuts, high precision and have a high dynamic range of operating materials. The consideration of this process to form thin-film flexible sensors with the metalized polymer films would have an edge due to their combined advantages. Also, it would reduce the time required to process each step in the entire fabrication process. The work done here explains the laser-inscribing of the metalized polymer films via selective scribing of the aluminum side.

Natural water bodies like rivers, sea, and streams consist of different kinds of minerals, including magnesium, sodium, zinc, etc. These minerals are present in certain ionic compounds such as oxides and sulfates at definite proportions. When the concentrations of these compounds increase beyond a certain level, it becomes disastrous for flora and fauna of the water bodies. For example, a high amount of sulfates in water can lead to a laxative effect leading to dehydration effects in infants [27]. Other developments with the rise in sulfate levels in the water bodies can result in anomalies in human bodies like intestinal discomfort and diarrhea. Thus, the World Health Organization has defined the safety levels of sulfate in water to be 250 ppm [28].

In order to maintain the consistency of the quality of natural water bodies, research work has been going on for some time. Even though the sensing of sulfate ions has been performed by different groups [29], [30], some drawbacks need to be addressed. For example, for the sensors that use selectivity, even though it increases the affinity towards the target molecule, the constant refreshing of the molecularly imprinted polymer layer becomes an issue regarding the time consumption and operation in harsh real-time conditions. In some cases like [29], certain associated disadvantages are their long analysis time, inaccuracy in the measurements, and a large amount of time required for fabrication. For the optical sensors that have been used for chemical sensing, some of the disadvantages associated with them are the interference of the ambient light with the operation of the sensors, limitation of long-term stability as a result of leaching, and limited dynamic range [30]. The cost of fabrication of the optical sensors is also very high, which discourages their usage in harsh conditions to restrict the physical damage. Again, none of these works describes the development of ready to use systems [31], [32]. Most of them have outlined the development of sensing prototypes, without mentioning the embedded signal-conditioning circuits. Therefore, there is an exact requirement of sensors to be used as an alternative for the low-cost, real-time detection of sulfate samples in water bodies. This is the first paper that describes the fabrication of low-cost, laser-inscribed sensors that have been characterized and integrated to form portable devices for the detection of sulfate ions in water bodies.

The paper has been subdivided into six sections. Section one gives a brief introduction about the significance of laser-inscribed PET sensors, along with the requirement of real-time systems for the on-chip detection of sulfates ions. While section two outlines the fabrication process of the sensor patches, sections three and four describe the working principle of the sensors and the experimental setup used for detection purposes, respectively. Section five explains the development of an IoT-based system, followed by section six, elucidating the experimental results related to impedance measurement and microcontroller-based sensing of different concentrations of sulfates ions. The conclusion is drawn in the final section of the paper.

II. FABRICATION OF THE SENSOR PATCHES

Figure 1 depicts the schematic diagram of the fabrication process followed to develop the sensor patches. The metalized PET films were attached to rectangular glass slides using biocompatible tapes (3M^{TM}VHB^{TM}) before they are taken to the laser platform for the inscription process. The glass slides were further connected to the platform to avoid their sideways movement during the laser-inscription process. The electrode patterns were made using CorelDraw X7, which was associated with the laser engraving machine as the design software. Metallized PET films (Tradekorea, HO-107) were used as the raw material for the inscription process. The aluminum side of the sensor can be differentiated from the polymer side based on higher electrical conductivity and smoothness of the former over the latter. The thicknesses of the metallic

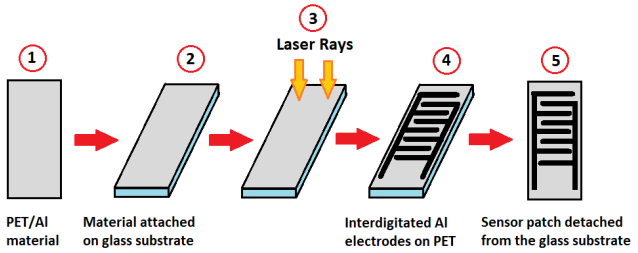

FIGURE 1. Schematic diagram of the fabrication steps of the laser-inscription metalized PET films. (1) After the attachment of the films on the (2) glass substrate, (3) the electrodes were formed on the sensors via laser- inscription. (4) Interdigitated electrodes were formed on the sensors (5) and subsequently peeled off the glass substrate for experimental purposes.

and polymeric sides were 300 and 500 microns, respectively. CO_2-based universal laser systems (Model: OLS 6.75 CO_2, spot diameter: 150 microns) were used for laser-inscription of the thin-films. The values for four laser parameters – power, speed, z-offset, and pulse per inch (PPI) – were adjusted to obtain the length, width, and interdigital distance of each electrode finger. Power (W) is defined as the energy exerted from the laser nozzle on the samples; speed decides the rate at which the nozzle moves over the samples; z-offset is used to adjust the focal point of the laser tip, and PPI decides the number of laser pulses being fired per inch on the laser-inscribed samples. This optimization was done by varying any one of the parameters at a specific time while keeping other parameters constant. The laser inscription process was carried out by exploiting the heat generated by the laser beam to form the electrodes. The intensity of this heat determined the attributes of the sensor. The selective scanning on the aluminum side was done in accordance with the electrode design assisted in the formation of electrode lines. The laser-parameters conjunctively moved the laser nozzle in the x-y direction to scan off the aluminum layer. The aluminum material from the shinier side curved off inversely to the design of the electrodes. This means that the aluminum metal stayed on the thin-films only in those regions of the electrode designs. The four laser parameters were fixed at certain optimized values, which included a power of 21 W, speed 30 m/min, 1.2 mm and PPI of 1000. These values were kept constant to selectively remove the aluminum material from the thinner side of the metalized polymer films.

Figure 2 shows the Zeiss confocal laser scanning a microscopic image of the width of a single electrode line. The formation was accompanied by the variation in the heat generated from the laser beam. Too much heat burnt the thin-films, whereas no or little heat created abrupt left no trace of the electrodes on the substrates. The reproducibility of these sensors was very high since identical values of the laser parameters were used to develop all the sensors. Figure 3 presents the top view of the Scanning Electron Microscope (SEM) image of the electrodes of the sensor patches. The rough surface refers to the aluminum electrodes in comparison to the smoother PET surface. It is seen that the electrode lines were prominent and perpendicular to the

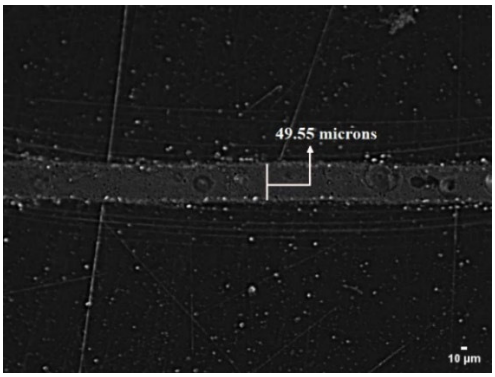

FIGURE 2. Microscopic image of a single electrode finger of the sensor.

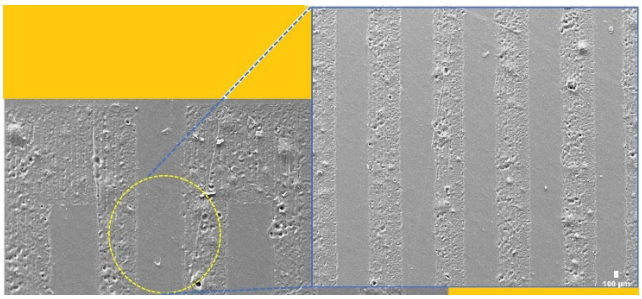

FIGURE 3. SEM image of the laser-inscription Al side showing the zoomed view of the electrode fingers.

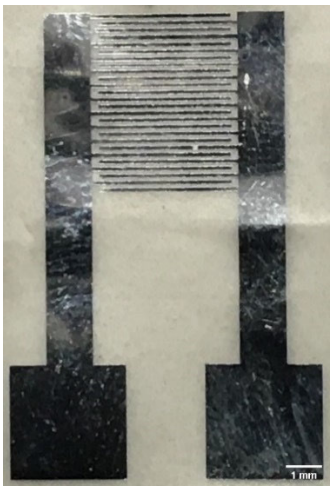

FIGURE 4. Top view of the developed sensor showing the aluminum side.

surface. The zoomed view shown in Figure 3 depicts the parallel nature of the electrode fingers. The heat generated by the laser caused molding and demolding of aluminum, which further created uneven cavities on the electrode fingers. Even though cavities were formed on the electrodes through the laser-inscription process, the change in the electrical conductivities of the sensors was negligible. After the fabrication process, the sensors were taken off the glass substrate and used for experimental procedures. Figure 4 depicts the top view of the finished product. More than three hundred prototypes were formed to validate the consistency of the parameters during the fabrication process.

Quick production of these laser-inscribed sensors was done, where around nine prototypes were fabricated within a span of two minutes. The length and the width of each interdigital finger were 1.2 cm and 50 microns, respectively. The interdigital distance between two consecutive electrode fingers was 375 microns. A pair of 12 interdigital electrode fingers were developed, with a total sensing area of 4.5 cm^2. The optimized values chosen for power, speed, z-offset and PPI for laser-inscription were 21 W, 30 m/min, 1.2 mm and 1000, respectively.

III. WORKING PRINCIPLE OF THE SENSOR PATCHES

The measuring principle of planar interdigital sensors is based on the interaction between a medium under test and an applied electric field between the electrodes [33]. Because the electric field penetrates the medium under test, electric displacement is produced inside it, which changes the charge stored between the electrodes and, consequently, the sensor capacitance. Therefore, changes in sensor capacitance allow conclusions to be drawn about the permittivity of the medium under test. Thus, the measurement of system parameters related to the permittivity of the medium is possible. Conventional parallel-plate capacitors work based on the same operating principle as planar capacitive sensors [34]. Between the two parallel electrodes, one demonstrating the driving electrode and the other signifying the sensing electrode, an electric field is formed uniformly [33]. Because of the much smaller thickness of the electrodes compared to the dimensions of the surface of the electrode, the fringing electric field is negligible. Since the electrodes are opened up in the case of a planar capacitive sensor, the fringing electric field becomes important, that is why this type of sensors are often mentioned as fringing electric field sensors in literature [33]–[36]. Even in the case of the planar capacitor, the electric field lines penetrate the monitored medium. Therefore, the sensor allows single-sided access to the medium, which is one of the most prominent benefits of planar capacitive sensors, as mentioned earlier. In order to make the sensor suitable for a particular application, the selection of sensor dimensions is critical as it is one of the main factors for sensor performance determination [37]. An appropriate configuration of a planar capacitive sensor is an interdigital electrode design, as the fringing electric field effect has the maximum contribution in sensor capacitance [38].

An interdigital electrode configuration includes two electrodes, one used as the sensing electrode and the other one used as the driving electrode. Both electrodes are usually formed by the same number of digits (fingers), each of which has a width w and is separated by a distance d. Another parameter generally used in interdigital electrode configurations is the spatial wavelength λ, which can be described as the gap between the centerlines of two consecutive fingers belonging to the same type of electrode and can be calculated using equation (1).

$$\lambda = 2.(w + d) \tag{1}$$

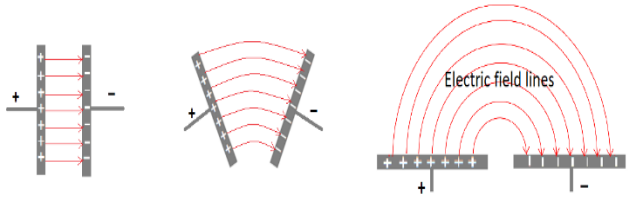

FIGURE 5. Working principle of the interdigital sensors depicting their planar nature. The characteristics of the electric field lines change when they are traveling from one electrode to another of opposite polarity due to their penetration through the MUT.

There is no unique description for the penetration depth, but one possible way to estimate it is to evaluate how deep the electric field enters the medium under test. That is why the thickness of the medium under test is increased until the point is touched, where 97 % of the capacitance is obtained. Besides the penetration depth, some other parameters are generally used to assess interdigital electrode structures such as signal strength, dynamic range, and measurement sensitivity [33], [34]. While the signal strength defines the output capacitance of a sensor for a medium under test with a certain thickness, the dynamic range shows the difference between the maximum capacitance for a medium under test and the capacitance in the absence of a medium. By minimizing the primary capacitance and maximizing the dynamic range, a maximum signal-to-noise ratio could be attained. The sensitivity of the sensor can be described as the ratio of the variation in the sensor output to the alteration in the system variable [36].

Figure 5 depicts the schematic diagram of the working principle of the sensors. The interdigital nature of the electrodes operated on a parallel-plate capacitive sensing mechanism. The planar nature of the electrodes assisted in carrying out a single-sided, non-invasive measurement process. The interdigitated fingers connected to the two connections were referred to as sensing and reference electrodes. When a time-dependent voltage signal was provided to the electrodes, the generated electric field would bulge from one electrode to another opposite polarity. Suppose any material is kept in contact or proximity to the sensing area of the patches. In that case, the electric field penetrates the material under test (MUT) while traveling from one electrode to another of opposite polarity. The height of this penetration depth can be optimized by determining the certain parameters linked to the structure of the fingers. Some of the studied parameters are the length and width of the interdigital electrodes and the distance between two electrodes of the same polarity. The characteristics of the electric field lines were studied to correspondingly determine the properties of the target material.

The repeatability of the interdigitated fingers helped amplify the output caused by the changing properties of the input parameters. Following the on-chip impedance testing and analysis of the fabricated sensors with the sulfate samples, both the resistive and capacitive electrical elements were found to have played a role in the change in the sensors'

response. The impedance (Z) of the sensors can be defined by equation (2), which comprises the resistive (R) and reactive (X) parts. This phenomenon can be studied using passive electrical parameters. The resistive part of the impedance changes due to both the solution resistance (R_S) of the samples and the charge-transfer resistance (R_{CT}) between the sensor and the sample. The change in the charge-transfer resistance leads to a corresponding change in the ionic current (I_C) flowing through the cell. The reactive part of the impedance also consists of two elements. Because of the capacitive nature of the interdigitated electrodes, a double layer capacitance (C_{DL}) is formed between the electrode-electrolyte interface. These four sensors decided the respective change in impedance, resistance, and reactance of the sensors, as shown in equation (3) and (4). Interdigital sensors have been used for a wide range of healthcare [39], [40], industrial [3], [4], [41], and environmental [42], [43] applications. Other advantages of these sensors include low cost of fabrication, simple operating principle, and low input power requirement.

$$Z = R + iX \tag{2}$$

For a small change in the resistive and reactive part of the impedance,

$$\frac{\Delta Z}{Z} = \frac{\Delta R}{R} + i\frac{\Delta X}{X} \tag{3}$$

Based on the three parameters as defined above,

$$\frac{\Delta Z}{Z} = \left(\frac{\Delta R_S}{R_s} + \frac{\Delta R_{CR}}{R_{CR}}\right) + i\frac{\Delta wC_{DL}}{wC_{DL}} \tag{4}$$

where,

$$|\boldsymbol{R}| = \sqrt{\left(\frac{\Delta \boldsymbol{R_S}}{\boldsymbol{R_S}}\right)^2 + \left(\frac{\Delta \boldsymbol{R_{CR}}}{\boldsymbol{R_{CR}}}\right)^2}, |\boldsymbol{C}| = \frac{\Delta \boldsymbol{wC_{DL}}}{\boldsymbol{wC_{DL}}}$$

IV. EXPERIMENTAL SETUP

Figure 6 shows the setup followed during the experimental procedure. On-chip impedance detection was carried out using these sensors. Due to the presence of dual electrodes on the sensors, the impedance spectroscopy technique was chosen for the detection and analysis purposes [44], [45]. The detection of the change in impedance was done in conjugation with the interdigital sensors to study their responses towards different samples. The sensors were attached to an acrylic sheet with tapes to prevent them from moving inside the solutions during experimentation. A HIOKI IM3536 High testing impedance analyzer was connected to the sensors to determine their output for every concentration and salt with regard to the change in frequency.

The sensors were connected through their bonding pads to the Kelvin probes of the impedance analyzer that were clamped above the sample solutions. The other end of the sensors, consisting of the sensing area, was immersed inside the solutions. The dipping of the sensing area of the patches

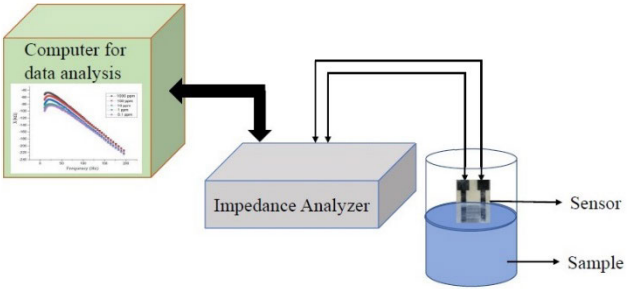

FIGURE 6. Schematic diagram to depict the experimental setup for the detection of sulfate concentrations in the water samples.

was done carefully to avoid the contact of the samples with either the bonding pads or the Kelvin probes. An alternating voltage of 10 mV was applied from the impedance analyzer as an input to the sensors. A small signal was chosen as a function of frequency to determine the real and imaginary part of the impedance. These small perturbations are used to drive the cell near the equilibrium condition [46]. The equilibrium nature is achieved through the ionic and faradic reactions in the medium. The small departures from equilibrium in terms of amplitude helps in obtaining a linear response. The impedance spectroscopy was carried at a wide range of frequencies at a single perturbation amplitude. The resistance and the reactance values were calculated concerning the change in frequency.

The impedance analyzer was connected to a laptop using a USB cable to collect the data on Microsoft Office Suite ® using an automated data acquisition algorithm. An average of three different responses was considered for each round to ensure the repeatability of the responses of the sensors. After each round, the sensors were washed and dried adequately before using them for the next round. Two different salts were tested, and their corresponding outputs were compared to determine the capability of the fabricated sensors to differentiate between them. Sodium Sulfate (Alfa Aesar, A19890) and DI were used as solutes and solvent, respectively, to form the solutions. Five different concentrations ranging between 0.1 ppm and 1000 ppm were developed for each of the molecular samples using serial dilution. An initial stock solution of 1000 ppm was initially formed by mixing 0.1 gm of the solute in 100 ml of DI water. Following the experiments with this sample, 10 ml of the previously formed solution with a concentration of 1000 ppm was mixed with 90 ml of DI water to form 100 ppm. This process was continued until the formation, and the testing of all the samples was completed.

V. IoT-BASED SYSTEM

The IoT-based portable system is useful to monitor water bodies' nutrients and record them regularly for observing the trends. We have also proposed a system which can record the sulfate data in any location and transfer them in real-time from a remote location. Figure 7 shows the block diagram that was used to carry out the IoT-based testing process. The central unit of the system was a microcontroller to test the

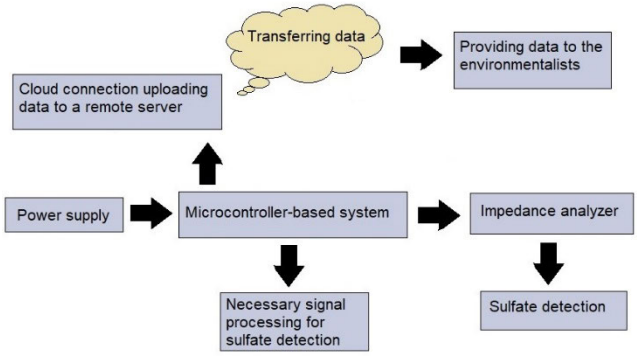

FIGURE 7. Block diagram of the microcontroller-based system used for testing the sulfate samples.

unknown sample and subsequently upload the data in the cloud server. The microcontroller was powered using a battery that was connected to the conditioning circuit. Arduino Uno Wi-Fi [47] was used as a microcontroller platform for data collection, analysis, and network communication. The Arduino Uno has integrated Wi-Fi connectivity, which provides instant wireless communication to the sensing system during the development phase.

The integrated Wi-Fi Module is a self-contained system on a chip (SoC) and has an integrated TCP/IP protocol stack that can provide access to any Wi-Fi network. AD5933 [48] is used as the impedance analyzer. It is a high precision impedance converter system solution that is used in other applications [40], [49]. The impedance analyzer is used to calibrate the sensor for various frequencies to identify the sensor characterization's operating frequency. Finally, the operating frequency is used to measure the unknown sulfate concentrations from any sample water. The I^2C protocol [50] was used to communicate between the microcontroller unit and the impedance analyzer. The working phenomenon of the sensing system is shown in Figure 8. The impedance analyzer requires to calibrate before every measurement to calculate the actual impedance of the sample. Therefore, we have used 2:1 multiplexer ADG849 to complete the initial calibration of the system. The calibration of the sensor is also done in the laboratory environment to measure the unknown samples. The calibration standard of sulfate is stored, and the system measures the impedance of the water to identify the concentration of sulfate. Once the measurement is done, this data was then uploaded to the IoT cloud server using a gateway to make it available for the monitoring unit. *Thingspeak* [51] was used to store this data in the cloud server.

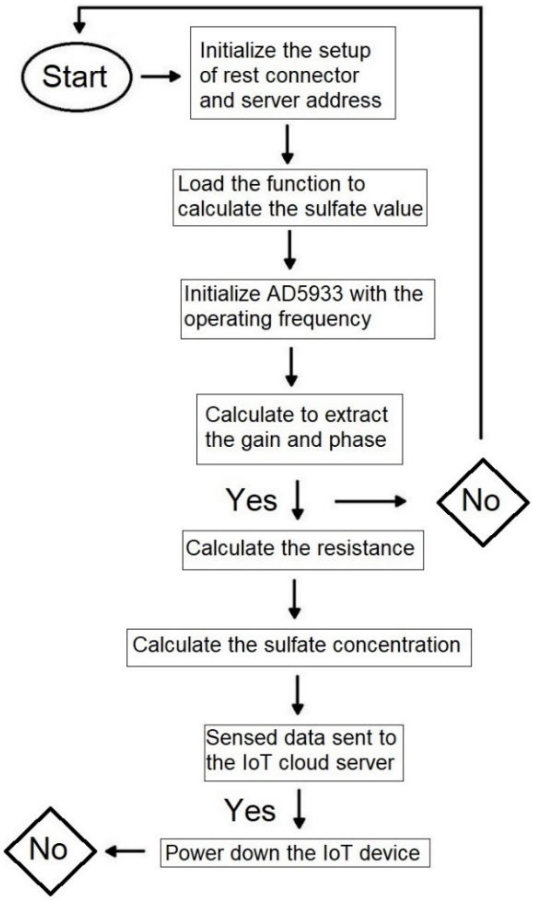

FIGURE 8. Flow chart of the proposed sensing system.

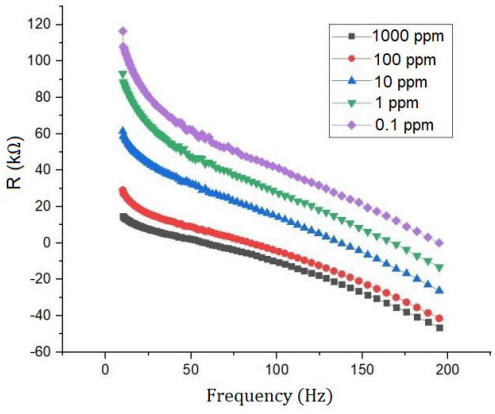

FIGURE 9. Response of the fabricated sensors towards sulfate samples for the resistive values.

VI. RESULTS AND DISCUSSIONS

Figures 9 and 10 represent the response of the sensor patches towards the sulfate samples. In order to cover the entire spectrum of low, safe and high levels of sulfate ions, the testing was done for concentrations ranging between 0.1 ppm and 1000 ppm. Although the frequency was swept between 10 Hz to 10 kHz, the results were considered between 10 Hz to 200 Hz due to their proper distinction within this range. It can be seen from Figures 9-10 that the sensor responds clearly to the five tested concentrations of the sulfate samples. The variation in the resistance and the reactance values are inversely proportioned to each other and to the tested concentrations. The behavior of the sensor inside the cell can be ascribed to the equivalent electrical parameters. Figure 11 shows the profiling of the sensor obtained through experiments conducted with one of the tested concentrations

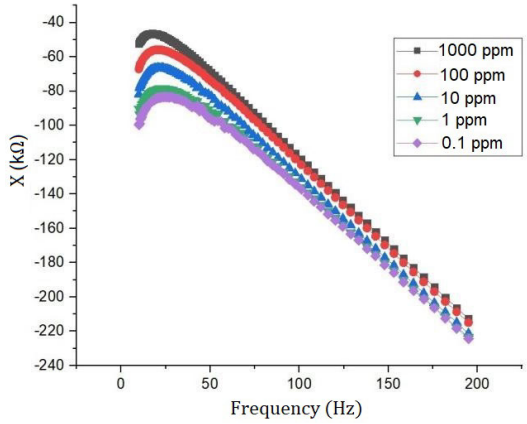

FIGURE 10. Response of the fabricated sensors towards sulfate samples for the reactive values.

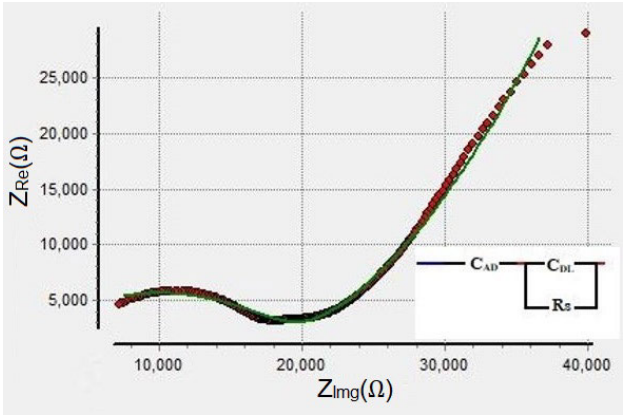

FIGURE 11. Profiling of the sensor done with one of the tested samples to determine the equivalent parameters of the prototypes.

(100 ppm) to evaluate the electrical parameters present in the fabricated prototypes. The evaluation of these parameters was done using a non-linear square curve fitting (CNLS) technique. This process operates on the electrochemical spectrum analyzer algorithm by making a comparative study between the experimental values and the theoretical response. One resistive and two capacitive elements were responsible for the change in the impedance values of the sensors.

Table 1 depicts the obtained electrical parameters, along with the error rate in their predictive values. The resistive part of the impedance varied as a result of changing solution resistance (Rs). With the increase in the ionic concentration of the samples, the corresponding flow of ionic current between the sensor and the solution increased. This led to a decrease in the resistance of the sensors. The corresponding change in the reactive values depends on the faradic current, which changes due to the two capacitive elements formed in the cell. The double-layered capacitance (C_{DL}) layer is formed at the electrode-electrolyte interface. In contrast, the adsorption capacitance (C_{AD}) is formed on the sensing area due to the nature of the patches' electrodes.

TABLE 1. Equivalent parameters of the circuit along with their values and error rate.

Equivalent electrical parameters	Values	Error rate (%)
Rs (kΩ)	4.29	3.89
C_{DL} (pF)	8.75	1.94
C_{AD} (pF)	72.12	0.14

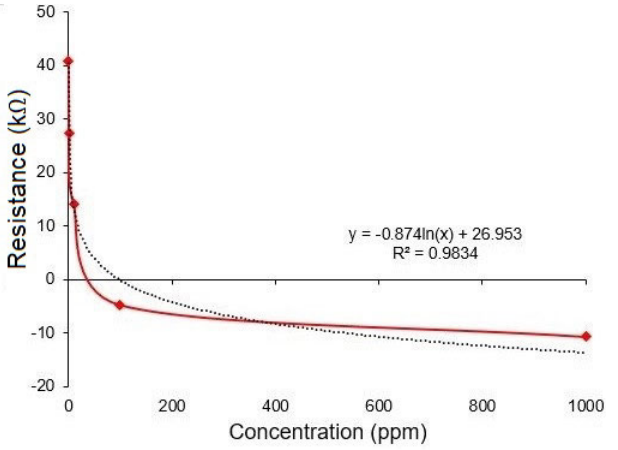

FIGURE 12. Comparison of sensitivities of the Al-PET sensors for the resistive readings. The five tested concentrations for sulfate samples were plotted against resistance for a frequency of 101.16 Hz.

The change in the adsorption capacitance depends on the variation in the number of ions that get adsorbed in the sensing area, which, in turn, depends on the particular tested concentration. One particular frequency was chosen from the swept frequency range to determine the sensitivity of the fabricated sensors towards the tested samples. Figure 12 shows the sensitivity of the developed sensors for a frequency of 101.16 Hz. The graph was plotted with the resistive values against the tested sulfate concentrations.

The frequency range was based on a logarithmic scale, considering their preparation through serial dilution. A logarithmic trend line was fitted to the plot to determine the sensitivity and determination coefficient (R^2). The R^2 value was obtained at 0.98, indicating that the resistances' experimental values were very close to the predictive values for the same. The sensitivity was 0.874 Ω/ppm, as obtained from the slope of the equations given in Figure 12. The sensors also had a quick response time of one second. The formula [52] used to calculate the limit of detection (LOD) of each type of sample is shown in equation (5). A concentration of 0.1 ppm was obtained as the LOD for the two types of ions.

$$LOD = \left(\frac{3S}{b}\right) \tag{5}$$

where, S is the standard deviation, b is the slope obtained from the standard curve.

The fabricated sensors had high efficiency in robustness, quick response, and a wide range of concentrations, which makes them suitable for different kinds of water bodies. These

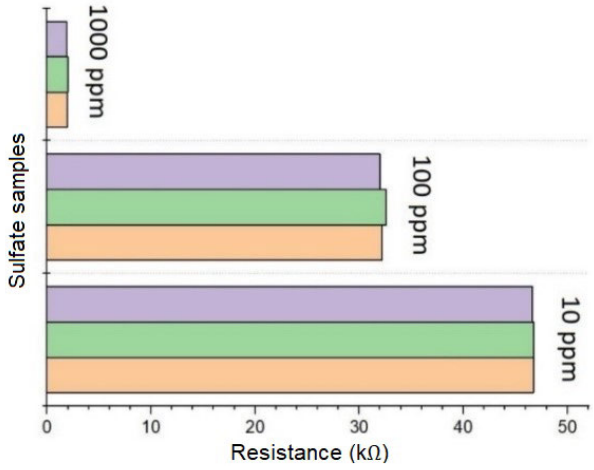

FIGURE 13. Repeatability of responses of the sensors for the sulfate samples for the tested concentrations of 1000, 100, and 10 ppm.

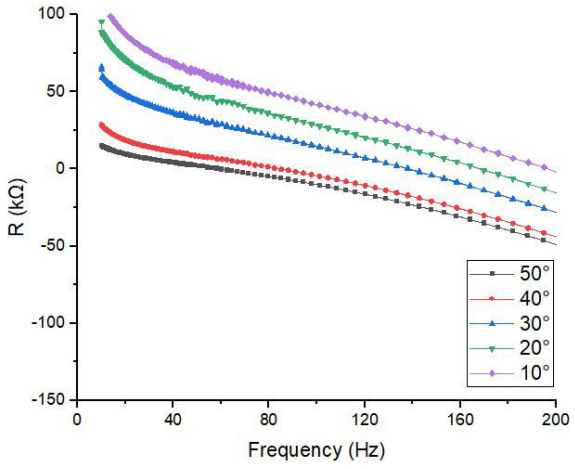

FIGURE 14. Response of the sensors with respect to the change in angles of the sensors at a particular concentration of 100 ppm.

sensors were also able to detect the ions in the samples with high accuracy and sensitivity. The next experiment was conducted to determine the repeatability of responses of the sensors for the two compounds. Figure 13 shows the response of the sensors with the outputs of each experiment conducted with three different concentrations. The samples were prepared by taking the water from reservoirs and spiking them with three concentrations of 1000 ppm, 100 ppm and 10 ppm.

After the first round of the experiment, the sensor was washed thoroughly with DI water, dried in the oven for five minutes, and then used in the next experiment. It can be seen that the sensors were capable of generating repeatable results for the tested concentrations. Due to the flexible characteristics of metalized polymer films, the sensors were also tested with different bending angles to analyze the differences in the responses with respect to its unbent or extended position. The experiments were conducted at a particular concentration of 100 ppm. Instead of acrylic sheets, the sensors were attached to flexible PET sheets. Figure 14 shows the change in resistance values with respect to frequency for

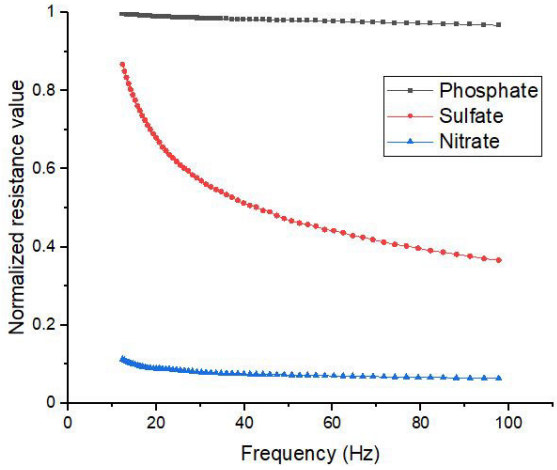

FIGURE 15. Comparison of the developed Al/PET sensors' interference studies for the sulfate, phosphate, and nitrate ions.

the five bending angles ranging between 10° and 50°. With the decrease in bending angles, the corresponding radius of curvature also decreases. This reduces the effective sensing area of the prototypes for electrochemical reactions to take place. As a result, the ionic current flowing between the sensor and solution reduces, thus increasing the resultant resistance. Although the sensors generated different results for different bending angles, the pattern or range of resistance values for the tested concentrations did not change too much.

Thus, it can be inferred that while operating in real-time situations, even if the prototypes become structurally distorted due to unknown reasons, the output values would not change much for the targeted samples. One of the significant phenomena of this sensor to target the ions present in water samples was their capability to distinguish the ions commonly present in salts. This was proven by conducting experiments with two other salts, including Ammonium Nitrate (Thermo Fisher Scientific, A676-500) and Potassium Phosphate (Sigma Aldrich, P5655). The concentrations for the three salts were fixed at 100 ppm to keep consistency with the previous experiment. Since the range of the output values obtained for the three salts were different, normalization was done on the output to fit the them one a single graph Figure 15 shows the response of the three salts with respect to frequency. It can be appreciated that the sensors are capable of distinguishing the output of the three target salts that are commonly present in water. The differences in the response of the sensors with respect to the three salts resulted due to the corresponding differences in the size of the salt ions. The resistive values of the three ions are arranged in the order, as shown in Figure 15, due to the larger size of phosphate (258 pm) ions in comparison to the sulfate (238 pm) and nitrate (179 pm) ions. Due to this, a higher amount of charge transfer takes place at the electrode-electrolyte interface for the phosphate ions than that of the other two ions. Table 2 shows a comparison between the performance of the developed prototypes and that of systems developed by other researchers for the detection of sulfate ions. This comparative

TABLE 2. Comparison between the present work and the performances of some of the significant examples done on the detection of sulfate ions.

Processed materials	Selectivity	Sensitivity	Stability	LOD	Advantages	Ref.
Piezoelectric crystals	Yes	85678 Hz dm^3 mol^{-1}	-	42 µmol dm^{-3}	• High precision in the response	[53]
Poly(vinyl chloride), zinc-phthalocyanine, hexadecyltrimethylammonium bromide	Yes	-29.2 mV/decade	High	1.0×10^{-6} M	• Fast response time • High reproducibility	[54]
Chromoionophore fluorescein octadecyl ether, Tridodecylmethyl ammonium chloride, bis-thiourea sulphate ionophore, polystyrene	Yes	0.025 Abs/µM	High	0.06 µM	• Wide linear range	[55]
Polyvinyl chloride, Trioctyl methyl ammonium chloride	Yes	–29.5 ± 0.5 mV/decade	High	1.0×10^{-8} M	• Fast response time • High reproducibility and long lifetime	[56]
Polyvinyl chloride, Trioctyl methyl ammonium chloride, bis(2-ethylhexyl)sebacate	Yes	-	High	1.8 x 10^{-9} M	• High reproducibility • Long lifetime	[57]
Al/PET	No	0.874 Ω/ppm	High	0.1 ppm	• High reproducibility • Fast response • Wide range of tested concentration	This work

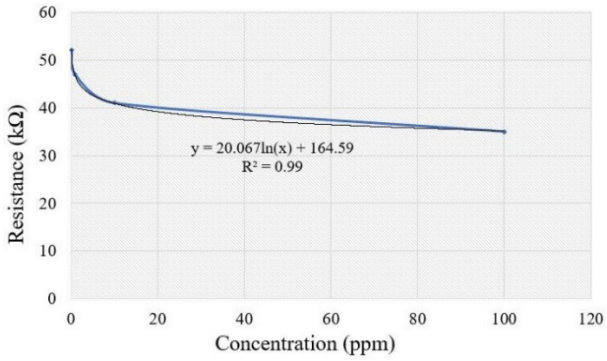

FIGURE 16. Standard curve developed from the data obtained from the measurements done by the microcontroller-based system.

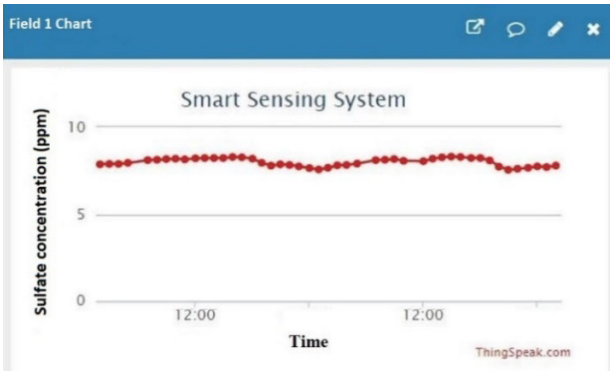

FIGURE 17. Real-time data obtained on the cloud server from the Wi-Fi embedded microcontroller.

study has been done on the basis of essential parameters that can determine the quality of the sensor.

It is observed that in addition to attributes provided by these flexible sensors, they are also capable of detecting sulfate ions with high efficiency. The frequency chosen to determine the sensitivity was rounded off (100 Hz) to set the microcontroller-based system's frequency. The calculated value was then processed by the embedded conditioning circuitry to evaluate the concentration from the sensitivity graph shown in Figure 12.

Figure 16 shows the standard curve obtained from the experiments done with the IoT-based proposed system. It can be concluded from the R^2 value that the predicted values were very close to that of the experimental values. The equation given in Figure 16 can be used to determine the sulfate concentration of an unknown sample. Figure 17 shows the real-time graph of the data that was transferred from the microcontroller-based system to the *Thingspeak* cloud server. The data was obtained from an unknown sulfate sample and simultaneously uploaded to the cloud server. The measurement concentration value of the new sulfate sample

was around 8 ppm. This value remained almost constant for two days, which shows the consistency of our proposed system.

VII. CONCLUSION

The design, fabrication, and implementation of IoT-based systems for environmental applications have been expressed in the paper. Among the various aspects that have been covered in the preceding sections, a few valuable points can be jotted down. Firstly, single-step fabrication can be done using the laser-scribing technique, which forms novel flexible sensors. The sensor prototypes were developed from metalized PET films. These sensors' advantages lie in the single-step fabrication process, simple operating principle, high conductivity of the electrodes, and multi-functionality. Secondly, the electrodes' interdigitated nature assisted in non-invasive, quick, single-sided measurements of two types of ions in the water samples. The sensors were employed to monitor different concentrations of sulfate samples. Each of the samples was prepared by mixing the individual salts to varying concentrations with DI water to form the respective aqueous solutions. The experimental results showed that the sensors could distinctively respond to each of these concentrations, thus validating their functionality for the chosen application. The sensors were capable of distinguishing each of the concentrations of the sulfate samples. The sensors had a response time of one second and a LOD of 0.1 ppm. The sensitivity of the sensors for the sulfate samples was 0.874 Ω/ppm. The sensors also showed high repeatability and stability in the responses. Finally, IoT-based systems were formed where the unknown samples were monitored through an impedance analyzer integrated into a Wi-Fi embedded microcontroller. The data was simultaneously monitored and uploaded to the cloud server. One of the issues that can be raised over this system is the absence of any selective layer for the sulfate ions. This can be resolved by considering the assistance of mathematical models to determine the presence of sulfate ions. The sensors' responses for any unknown samples in the water bodies can be classified using statistical tools like the principal component analysis (PCA) technique to determine their correlation to a particular set of concentrations. The error percentages in these impedance values can be cross-checked via classifying the impedance values into specific sets to determine the range of concentrations. Further work would be done to optimize the developed sensing systems for measuring the presence of other interfering molecules in the water samples. Analysis of the promote control will be done to develop IoT-based systems that would be capable of performing autonomously on real-time scenarios.

ACKNOWLEDGMENT

(Shan He and Shilun Feng contributed equally to this work.)

REFERENCES

[1] N. Yamazoe, G. Sakai, and K. Shimanoe, "Oxide semiconductor gas sensors," *Catal. Surv. Asia*, vol. 7, no. 1, pp. 63–75, Apr. 2003.

[2] S. Soloman, *Sensors Handbook*. New York, NY, USA: McGraw-Hill, 2009.

[3] A. Nag, A. I. Zia, X. Li, S. C. Mukhopadhyay, and J. Kosel, "Novel sensing approach for LPG leakage detection: Part I—Operating mechanism and preliminary results," *IEEE Sensors J.*, vol. 16, no. 4, pp. 996–1003, Feb. 2016.

[4] A. Nag, A. I. Zia, X. Li, S. C. Mukhopadhyay, and J. Kosel, "Novel sensing approach for LPG leakage detection—Part II: Effects of particle size, composition, and coating layer thickness," *IEEE Sensors J.*, vol. 16, no. 4, pp. 1088–1094, Feb. 2016.

[5] X. Liu, M. Mwangi, X. Li, M. O'Brien, and G. M. Whitesides, "Based piezoresistive MEMS sensors," *Lab Chip*, vol. 11, no. 13, pp. 2189–2196, 2011.

[6] R. Bogue, "MEMS sensors: Past, present and future," *Sensor Rev.*, vol. 27, no. 1, pp. 7–13, Jan. 2007.

[7] Y. Unno, A. A. Affolder, P. P. Allport, R. Bates, C. Betancourt, J. Bohm, H. Brown, C. Buttar, J. R. Carter, G. Casse, and H. Chen, "Development of n-on-p silicon sensors for very high radiation environments," *Nucl. Instrum. Methods Phys. Res. A, Accel. Spectrom. Detect. Assoc. Equip.*, vol. 636, no. 1, pp. S24–S30, 2011.

[8] R. G. Azevedo, J. Zhang, D. G. Jones, D. R. Myers, A. V. Jog, B. Jamshidi, M. B. J. Wijesundara, R. Maboudian, and A. P. Pisano, "Silicon carbide coated MEMS strain sensor for harsh environment applications," in *Proc. IEEE 20th Int. Conf. Micro Electro Mech. Syst. (MEMS)*, Jan. 2007, pp. 643–646.

[9] A. Nag, S. C. Mukhopadhyay, and J. Kosel, "Wearable flexible sensors: A review," *IEEE Sensors J.*, vol. 17, no. 13, pp. 3949–3960, Jul. 2017.

[10] A. Nag, S. C. Mukhopadhyay, and J. Kosel, "Flexible carbon nanotube nanocomposite sensor for multiple physiological parameter monitoring," *Sens. Actuators A, Phys.*, vol. 251, pp. 148–155, Nov. 2016.

[11] *Disadvantages of Silicon Sensors*. Accessed: Dec. 3, 2020. [Online]. Available: https://www.printedelectronicsworld.com/articles/52/problems-with-silicon-chips

[12] *Advantages and Disadvantages of Silicon*. Accessed: Dec. 3, 2020. [Online]. Available: http://www.rfwireless-world.com/Terminology/Advantages-and-Disadvantages-of-Silicon.html

[13] A. Nag, S. Feng, S. C. Mukhopadhyay, J. Kosel, and D. Inglis, "3D printed mould-based graphite/PDMS sensor for low-force applications," *Sens. Actuators A, Phys.*, vol. 280, pp. 525–534, Sep. 2018.

[14] A. Nag, N. Afasrimanesh, S. Feng, and S. C. Mukhopadhyay, "Strain induced graphite/PDMS sensors for biomedical applications," *Sens. Actuators A, Phys.*, vol. 271, pp. 257–269, Mar. 2018.

[15] A. Nag, S. C. Mukhopadhyay, and J. Kosel, "Tactile sensing from laser-ablated metallized PET films," *IEEE Sensors J.*, vol. 17, no. 1, pp. 7–13, Jan. 2017.

[16] U. Yaqoob, D.-T. Phan, A. S. M. I. Uddin, and G.-S. Chung, "Highly flexible room temperature NO_2 sensor based on MWCNTs-WO_3 nanoparticles hybrid on a PET substrate," *Sens. Actuators B, Chem.*, vol. 221, pp. 760–768, Dec. 2015.

[17] Y. Qin, Q. Peng, Y. Ding, Z. Lin, C. Wang, Y. Li, F. Xu, J. Li, Y. Yuan, X. He, and Y. Li, "Lightweight, superelastic, and mechanically flexible Graphene/Polyimide nanocomposite foam for strain sensor application," *ACS Nano*, vol. 9, no. 9, pp. 8933–8941, Sep. 2015.

[18] J. A. Dobrzynska and M. A. M. Gijs, "Flexible polyimide-based force sensor," *Sens. Actuators A, Phys.*, vol. 173, no. 1, pp. 127–135, Jan. 2012.

[19] Y. Wang, X. Wang, W. Lu, Q. Yuan, Y. Zheng, and B. Yao, "A thin film polyethylene terephthalate (PET) electrochemical sensor for detection of glucose in sweat," *Talanta*, vol. 198, pp. 86–92, Jun. 2019.

[20] M. A. Zulkifley, M. M. Mustafa, A. Hussain, A. Mustapha, and S. Ramli, "Robust identification of polyethylene terephthalate (PET) plastics through Bayesian decision," *PLoS ONE*, vol. 9, no. 12, Dec. 2014, Art. no. e114518.

[21] B. S. Makki, M. Kargar, S. Mohajerzadeh, T. Maleki, and D. Shahrjerdi, "Application of PET plastics in micro-sensor fabrication," in *Proc. 12th IEEE Int. Conf. Fuzzy Syst.*, Dec. 2003, pp. 357–360.

[22] *Creative Process for the High-Barrier Metalized Films*. Accessed: Dec. 3, 2020. [Online]. Available: https://www.cosmofilms.com/blog/creative-process-for-the-high-barrier-metalized-films/

[23] *Metallized PET-Film*. Accessed: Dec. 3, 2020. [Online]. Available: https://alfipa.com/products/aluminum-foil-metalized-pet-film/

[24] *The Advantages of Laser Cutting*. Accessed: Dec. 3, 2020. [Online]. Available: https://www.spilasers.com/application-cutting/the-advantages-of-laser-cutting/

[25] H. Tian, Y. Shu, Y. L. Cui, W. T. Mi, Y. Yang, D. Xie, and T. L. Ren, "Scalable fabrication of high-performance and flexible graphene strain sensors," *Nanoscale*, vol. 6, no. 2, pp. 699–705, 2014.
[26] V. Strong, S. Dubin, M. F. El-Kady, A. Lech, Y. Wang, B. H. Weiller, and R. B. Kaner, "Patterning and electronic tuning of laser scribed graphene for flexible all-carbon devices," *ACS Nano*, vol. 6, no. 2, pp. 1395–1403, Feb. 2012.
[27] *Sulfate Safety Levels*, Water Res. Center, B.F. Environ. Consultants, Dallas, PA, USA. [Online]. Available: https://water-research.net/index.php/sulfates
[28] *Sulphate Levels*. Accessed: Dec. 3, 2020. [Online]. Available: https://www.canada.ca/en/health-canada/services/publications/healthy-living/guidelines-canadian-drinking-water-quality-guideline-technical-document-sulphate.html
[29] A. S. M. Nor, M. Faramarzi, M. A. M. Yunus, and S. Ibrahim, "Nitrate and sulfate estimations in water sources using a planar electromagnetic sensor array and artificial neural network method," *IEEE Sensors J.*, vol. 15, no. 1, pp. 497–504, Jan. 2015.
[30] H. Qazi, A. Mohammad, and M. Akram, "Recent progress in optical chemical sensors," *Sensors*, vol. 12, no. 12, pp. 16522–16556, Nov. 2012.
[31] C. Parolo and A. Merkoçi, "Based nanobiosensors for diagnostics," *Chem. Soc. Rev.*, vol. 42, no. 2, pp. 450–457, 2013.
[32] A. T. Singh, D. Lantigua, A. Meka, S. Taing, M. Pandher, and G. Camci-Unal, "Based sensors: Emerging themes and applications," *Sensors*, vol. 18, no. 9, p. 2838, 2018.
[33] X. Hu and W. J. S. R. Yang, "Planar capacitive sensors-designs and applications," School Elect. Electron. Eng., Univ. Manchester, Manchester, U.K., Tech. Rep., 2010.
[34] A. V. Mamishev, K. Sundara-Rajan, F. Yang, Y. Du, and M. Zahn, "Interdigital sensors and transducers," *Proc. IEEE*, vol. 92, no. 5, pp. 808–845, May 2004.
[35] R. N. Dean, A. K. Rane, M. E. Baginski, J. Richard, Z. Hartzog, and D. J. Elton, "A capacitive fringing field sensor design for moisture measurement based on printed circuit board technology," *IEEE Trans. Instrum. Meas.*, vol. 61, no. 4, pp. 1105–1112, Apr. 2012.
[36] J. Döring, L. Tharmakularajah, and K.-L. Krieger, "P2.7 study of interdigital electrode structures for the detection of water spray," in *Proc. Tagungsband*, 2019, pp. 700–707.
[37] X. B. Li, S. D. Larson, A. S. Zyuzin, and A. V. Mamishev, "Design principles for multichannel fringing electric field sensors," *IEEE Sensors J.*, vol. 6, no. 2, pp. 434–440, Apr. 2006.
[38] J. Mizuguchi, J. C. Piai, J. A. de Franca, M. B. de Morais Franca, K. Yamashita, and L. C. Mathias, "Fringing field capacitive sensor for measuring soil water content: Design, manufacture, and testing," *IEEE Trans. Instrum. Meas.*, vol. 64, no. 1, pp. 212–220, Jan. 2015.
[39] A. R. M. Syaifudin, A. I. Zia, S. C. Mukhopadhyay, P. L. Yu, C. P. Gooneratne, and J. Kosel, "Improved detection limits of bacterial endotoxins using new type of planar interdigital sensors," in *Proc. IEEE Sensors*, Oct. 2012, pp. 1–4.
[40] N. Afsarimanesh, M. E. E. Alahi, S. C. Mukhopadhyay, and M. Kruger, "Development of IoT-based impedometric biosensor for point-of-care monitoring of bone loss," *IEEE J. Emerg. Sel. Topics Circuits Syst.*, vol. 8, no. 2, pp. 211–220, Jun. 2018.
[41] A. Nag and S. C. Mukhopadhyay, "Fabrication and implementation of printed sensors for taste sensing applications," *Sens. Actuators A, Phys.*, vol. 269, pp. 53–61, Jan. 2018.
[42] M. E. E. Alahi, A. Nag, S. C. Mukhopadhyay, and L. Burkitt, "A temperature-compensated graphene sensor for nitrate monitoring in real-time application," *Sens. Actuators A, Phys.*, vol. 269, pp. 79–90, Jan. 2018.
[43] A. Nag, S. C. Mukhopadhyay, and J. Kosel, "Sensing system for salinity testing using laser-induced graphene sensors," *Sens. Actuators A, Phys.*, vol. 264, pp. 107–116, Sep. 2017.
[44] N. I. Ramli, N. A. B. Ismail, F. Abd-Wahab, and W. W. A. W. Salim, "Cyclic Voltammetry and electrical impedance spectroscopy of electrodes modified with PEDOT: PSS-reduced graphene oxide composite," in *Transparent Conducting Films*. London, U.K.: IntechOpen, 2018.
[45] N. A. Batrisya Ismail, F. Abd-Wahab, and W. W. Amani Wan Salim, "Cyclic voltammetry and electrochemical impedance spectroscopy of partially reduced graphene Oxide–PEDOT:PSS transducer for biochemical sensing," in *Proc. IEEE-EMBS Conf. Biomed. Eng. Sci. (IECBES)*, Dec. 2018, pp. 330–335.
[46] *Impedance Basics*. Accessed: Dec. 3, 2020. [Online]. Available: https://www.cei.washington.edu/wp-content/uploads/2018/05/EIS-and-NLEIS-Wiki.pdf
[47] Arduino. (Jun. 8, 2020). *ARDUINO UNO WIFI REV2*. Accessed: Dec. 3, 2020. [Online]. Available: https://store.arduino.cc/usa/arduino-uno-wifi-rev2
[48] A. Devices. (Jun. 8, 2020). *1 MSPS, 12-Bit Impedance Converter, Network Analyzer*. Accessed: Dec. 3, 2020. [Online]. Available: https://www.analog.com/media/en/technical-documentation/data-sheets/AD5933.pdf
[49] M. E. E. Alahi, N. Pereira-Ishak, S. C. Mukhopadhyay, and L. Burkitt, "An Internet-of-Things enabled smart sensing system for nitrate monitoring," *IEEE Internet Things J.*, vol. 5, no. 6, pp. 4409–4417, Dec. 2018.
[50] S. E. (Jun. 8, 2020). I2C. Accessed: Dec. 3, 2020. [Online]. Available: https://learn.sparkfun.com/tutorials/i2c/all
[51] *Thingspeak*. Accessed: Oct. 5, 2020. [Online]. Available: https://thingspeak.com/
[52] A. Shrivastava and V. Gupta, "Methods for the determination of limit of detection and limit of quantitation of the analytical methods," *Chronicles Young Scientists*, vol. 2, no. 1, p. 21, 2011.
[53] L. V. L. Venâncio, A. S. F. Farinha, and M. T. S. R. Gomes, "Analysing sulphate and chloride in mineral drinking water by flow injection analysis with a single acoustic wave sensor," *Talanta*, vol. 189, pp. 65–70, Nov. 2018.
[54] M. R. Ganjali, M. R. Pourjavid, M. Shamsipur, T. Poursaeri, M. Rezapour, M. Javanbakht, and H. Sharghi, "Novel membrane potentiometric sulfate ion sensor based on zinc-phthalocyanine for the quick determination of trace amounts of sulfate," *Anal. Sci.*, vol. 19, no. 7, pp. 995–999, 2003.
[55] T. Guinovart, P. Blondeau, and F. J. Andrade, "Sulphate-selective optical microsensors: Overcoming the hydration energy penalty," *Chem. Commun.*, vol. 51, no. 52, pp. 10377–10380, 2015.
[56] M. Mazloum Ardakani, Z. Akrami, M. Mansournia, and H. R. Zare, "Sulfate-selective electrode based on a complex of copper," *Anal. Sci.*, vol. 22, no. 5, pp. 673–678, 2006.
[57] *Sulphate Ion Selective Electrodes*. Accessed: Dec. 3, 2020. [Online]. Available: https://shodhganga.inflibnet.ac.in/bitstream/10603/31656/13/14_chapter%206.pdf

SHAN HE received the Ph.D. degree in food science and technology from Flinders University, Australia. His career trajectory crossed both academic and industry, and three continents (Australia in Oceania, China in Asia, and Italy in Europe). He is currently an Associate Professor with Guangzhou University, China. His research interests include variety of food research areas, such as advanced food processing, protein hydrolyzation, emulsion, connecting the newly emerged technologies, such as sensors, artificial intelligence, and block chain, with conventional food technologies.

SHILUN FENG received the master's degree in biomedical microelectromechanical systems (Bio-MEMS) from the Department of Micro and Nano Systems Technology (IMST), Buskerud and Vestfold University College (HBV), Tønsberg, Norway, and the Ph.D. degree in biomedical POCT microfluidics with Dr. David Inglis, specialised in POCT microfluidic sampling probe and POCT on-chip cell concentrator, from the School of Engineering, Faculty of Science and Engineering, Macquarie University, Australia. He is focusing on different point-of-care testing (POCT) researches for food, environmental water, and biomedical sensing. He is currently an Associate Professor with the State Key Laboratory of Transducer Technology, Shanghai Institute of Microsystem and Information Technology, Chinese Academy of Sciences, Shanghai. He is cooperating with Prof. Shan He and Dr. Anindya Nag for the POCT devices on food research. He just finished his Research Fellow journal for POCT microfluidics projects on environmental water with the School of Electrical and Electronic Engineering, Nanyang Technological University, Singapore. He also cooperated with Dr. Anindya Nag and Professor Subhas Mukhopadhyay for the POCT wearable sensing devices. He was developing the POCT devices for the urinary tract infections disease for elderly people. His research interests include biomedical microfluidics, microfabrication, simulation and modeling, and point-of-care (POC) sampling, manipulation and testing with the developments of biodevice and instrumentation systems.

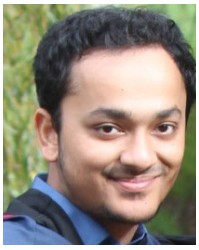

ANINDYA NAG (Member, IEEE) received the B.Tech. degree from the West Bengal University of Technology, India, in 2013, the M.S. degree from Massey University, New Zealand, in 2015, and the Ph.D. degree from Macquarie University, Australia, in 2018. From February 2019 to August 2020, he has worked as a Lecturer with the Dongguan University of Technology, China. He is currently working as a Postdoctoral Student with the King Abdullah University of Science and Technology, Thuwal, Saudi Arabia. His paper, Wearable Flexible Sensors, has been one of the top 25 downloaded papers in the IEEE Sensor Journal, from June 2017 to September 2018. He has authored or coauthored over 50 research articles, different journal articles, conference proceedings, and book chapters. His research interests include MEMS, flexible sensors, printing technology, and nanotechnology-based smart sensors for health, environmental and industrial monitoring applications.

NASRIN AFSARIMANESH received the Bachelor of Technology degree in electronics from Islamic Azad University, Iran, in 2006, the master's degree in electronics from the University of Pune, India, in 2010, and the Ph.D. degree from the Department of Engineering, Faculty of Science and Engineering, Macquarie University, Australia, in November 2018. Since September 2019, she has been a Lecturer with the DCI-CNAM Institute, Dongguan University of Technology, Guangdong, China. Her research interests include MEMS-based sensors and smart sensing systems.

MD. ESHRAT E ALAHI (Member, IEEE) received the Ph.D. degree in electronic engineering from Macquarie University, Sydney, NSW, Australia, and the M.Sc. degree in information and automation engineering from the University of Bremen, Germany. During his Ph.D. research, he developed capacitive interdigital sensors to detect nitrate as contamination in water. He is currently working as a Postdoctoral Research Fellow with the Shenzhen Institute of Advanced Technology (SIAT), Chinese Academy of Sciences. He has got research funds from the Chinese Academy of Sciences (CAS) and the National Natural Science Foundation of China (NSFC) as a Principal Investigator (PI). He has published more than 35 research papers, including SCI journals, conference proceedings, and book chapters. His research interests include sensor design and fabrication for water quality measurement, nano energy, robust neural interface, and neural recording/stimulation device for biomedical applications.

SIYING LI is currently pursuing the master's degree in food science and technology with Guangzhou University. Her supervisor is Associate Prof. Shan He, the first author of this manuscript. Her project is regarding the advanced processing development in Kombucha production, including the section of sensor development to determine the quality of kombucha in real time during production.

SUBHAS CHANDRA MUKHOPADHYAY (Fellow, IEEE) received the B.E.E. (Hons.), M.E.E., Ph.D. degrees in India and the D.Eng. degree in Japan. He has over 30 years of teaching, industrial, and research experience. He is currently a Professor of mechanical/electronics engineering with Macquarie University, Australia, and the Discipline Leader of the Mechatronics Engineering Degree Programme. He has supervised over 40 postgraduate students and over 100 Honours students. He has examined over 60 postgraduate theses. He has published over 400 papers in different international journals and conference proceedings, authored nine books and 42 book chapters, and edited 18 conference proceedings. He has also edited 32 books with Springer Verlag and 25 journal special issues. He has delivered 355 presentations, including keynote, invited, tutorial, and special lectures. His current research interests include smart sensors and sensing technology, instrumentation techniques, wireless sensors and network (WSN), the Internet of Things (IoT), and so on. He is a Fellow of IET, U.K., and IETE, India. He has organized over 20 international conferences as either General Chair/Co-Chair or Technical Programme Chair. He chairs the IEEE NSW Sensors Council chapter. He is a Topical Editor of the IEEE Sensors Journal. He is also an Associate Editor of the IEEE Transactions on Instrumentation and Measurements. He is a Distinguished Lecturer of the IEEE Sensors Council, during 2017–2022.

JONATHAN WOON CHUNG WONG received the Ph.D. degree in environmental science from Murdoch University, Western Australia. He is currently a Professor with the Department of Biology, Hong Kong Baptist University, where he has taught, since 1992. He is also the Director of the Sino-Forest Applied Research Centre for Pearl River Delta Environment and Hong Kong Organic Resource Centre. Over the years, he has conducted researches exploring the reutilization of organic wastes for energy and biomass production, developing innovative composting technology, anaerobic digestion of food waste, and sewage sludge treatment. Over the years, he has received over HK$150 million of research funding and published over 400 SCI publication and conference proceedings. He was bestowed with Medal of Honor by the Government of Hong Kong Special Administrative Region, in 2011, for his service and contribution to the Environment, and appointed as Justice of Peace, in 2014.